Journal of Guidance, Control, and Dynamics
Vol. 42, No. 11, November 2019

Nonlinear Optimal Guidance for Intercepting a Stationary Target

Zheng Chen*
Zhejiang University, 310027 Hangzhou, Zhejiang, China
and
Tal Shima†
Technion–Israel Institute of Technology, 3200003 Haifa, Israel

DOI: 10.2514/1.G004341

The problem of optimally guiding an interceptor to a stationary target is studied in a nonlinear setting. First of all, it is shown that a global solution does not exist for the typical free-time minimum-effort nonlinear optimal intercept problem. This leads to consideration of the linear combination of the control effort and engagement duration as the objective function. The necessary conditions for the optimal intercept problem with the new objective function are found to be parameterized by a scalar, reducing the problem of deriving the optimal guidance law to the problem of finding the zeros of a real-valued function. Moreover, a semianalytical form for the real-valued function is devised, and the interval for its zeros is restricted, allowing the use of a brute-force search to efficiently find all the zeros. As a result, the nonlinear optimal guidance law can be efficiently established. Finally, the characteristics of the guidance law are exemplified and studied through simulations, showing that the nonlinear optimal guidance law performs better than the conventional proportional navigation, especially for cases with large initial heading errors.

I. Introduction

THE problem of designing guidance laws for a pursuer to intercept a stationary target has been extensively studied since the 1960s. Such guidance laws are generally derived by linearizing the engagement around a nominal collision course [1–5]. This linearization allows us to use the linear-quadratic optimal control method to establish optimal guidance laws. For instance, proportional navigation (PN), which was initially derived from physical intuition and is probably the most popular intercept guidance law, was shown to be optimal in terms of control effort [6,7] in the linearized setting. Nevertheless, once the deviations from the collision triangle are relatively large, the linearization is not valid, and hence PN does not preserve the optimality any more.

In the nonlinear setting, some quantitative analyses of the nonlinear guidance problem were presented in Ref. [8] along with some comparisons to PN. By introducing a time-varying weighting factor into the control effort, the optimality of PN was studied in Ref. [9] without any linearization. The analyses in Ref. [9] showed that PN with any constant navigation gain can be equivalent to the nonlinear optimal guidance if the cost function is not the control effort itself but weighted by an appropriate time-varying weighting function. It is worth mentioning that, in the nonlinear setting, the optimal intercept guidance law is usually analyzed or derived by minimizing the control effort of the pursuer with a free final time (see, e.g., Ref. [8]).

In this paper, we shall show that the free-time nonlinear problem of intercepting a stationary target with purely minimizing control effort, which is the same as the one considered in Ref. [8], is not a well-posed optimal control problem (cf. Theorem 1). This leads us to consider the linear combination of the control effort and engagement duration as the objective function. Because a global optimum exists for the optimal intercept problem with the new objective function (cf. Theorem 2), the corresponding necessary conditions for optimality are analyzed in this paper to derive the nonlinear optimal intercept guidance.

In fact, the optimal intercept problem with the new objective function was studied in Refs. [10,11]. It was shown in Ref. [10] that the closed-form guidance law in the nonlinear setting was not available and that the optimal guidance law could be obtained by numerically solving a set of three nonlinear equations with three unknown variables. It should be noted that a set of multiple nonlinear equations may have more than one root, and a numerical solver generally cannot find all the zeros. Therefore, the developments in Ref. [10] could not guarantee the solution (found by a numerical solver) to be the optimal guidance law unless all local solutions corresponded to the same global minimum. In Ref. [11], the optimal intercept problem with the new objective function was solved by combining the genetic algorithm with the shooting method, and the computed solution was used to analyze an all-aspect near-optimal guidance law that was developed in Ref. [11]. By discretizing the nonlinear optimal control problem to formulate a nonlinear programming problem, a successive convex optimization approach in a recent work [12] was employed to compute the optimal intercept guidance law. However, the solution found either by the combined genetic algorithm-shooting method in Ref. [11] or by the successive convex optimization in Ref. [12] cannot be guaranteed to be the global solution because both approaches converge to local solutions.

Unlike Refs. [10–12], this paper aims to synthesize the solution for the optimal nonlinear intercept problem so that the nonlinear guidance law can be efficiently established. To be specific, we show that the necessary conditions from Pontryagin's maximum principle are parameterized by a scalar. As a result of the parameterization, it is found that the optimal guidance law is an analytical function in terms of the zeros of a real-valued function. This reduces the problem of deriving the optimal guidance law to the problem of finding the zeros of a real-valued function. In addition, some geometric properties for the optimal solution are established. By using those properties, we are able to devise a semianalytical form for the real-valued function and to restrict the intervals of its zeros. To this end, a brute-force search can be used to efficiently find all the zeros of the real-valued function, which finally gives rise to the nonlinear optimal feedback guidance law.

This paper is organized as follows. In Sec. II, the optimal nonlinear intercept problem is formulated and the necessary conditions for optimality are presented. In Sec. III, the necessary conditions are parameterized and some geometric properties for the optimal solution are established, showing that the optimal guidance law is determined by the zeros of a real-valued function. In Sec. IV, a semianalytical form is devised for the real-valued function and the intervals of its

Received 17 January 2019; revision received 26 April 2019; accepted for publication 7 May 2019; published online 17 June 2019.

*Researcher, School of Aeronautics and Astronautics; z-chen@zju.edu.cn. Member AIAA.

†Professor, Faculty of Aerospace Engineering; tal.shima@technion.ac.il. Associate Fellow AIAA.

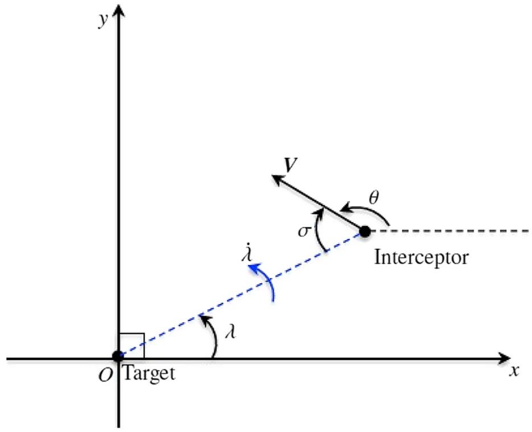

Fig. 1 Two-dimensional intercept geometry.

zeros are restricted so that a brute-force search can be used to find all the zeros. Finally, some numerical simulations in Sec. V demonstrate the viability of the approach presented in this paper.

II. Problem Formulation

In this section, the optimal control problem of intercepting a stationary target is formulated, and its necessary conditions for optimality are presented by applying Pontryagin's maximum principle.

A. Optimal Intercept Problem

Consider the two-dimensional geometry of the stationary target intercept problem, which is presented in Fig. 1. The origin of frame Oxy is located at the target, the x axis points to the initial position of the interceptor, and the y axis is defined by rotating the x axis 90 deg counterclockwise. Throughout the paper, we denote by $(x, y) \in \mathbb{R}^2$ the position of the interceptor in frame Oxy, and we denote by $\theta \in [-\pi, \pi]$ the angle between the x axis and the velocity vector $\boldsymbol{V}$ of the interceptor. The angle θ is usually called the heading angle of the interceptor, and it is positive when measured counterclockwise. The line of sight (LOS) from the interceptor to the target makes an angle of λ with the x axis, and this angle is positive if measured counterclockwise. We will use $\dot{\lambda}$ to denote the LOS rate. The angle σ between the LOS and the velocity vector $\boldsymbol{V}$ is called the look angle, which is positive when measured clockwise. By normalizing the magnitude of the velocity $\boldsymbol{V}$ of the interceptor to one, the nonlinear kinematics of the interceptor is represented by

$$(\Sigma)\colon \begin{cases} \dot{x}(t) = \cos\theta(t), \\ \dot{y}(t) = \sin\theta(t), \\ \dot{\theta}(t) = u(t) \end{cases} \tag{1}$$

where $t > 0$ is the time, the dot denotes the differentiation with respect to time, and $u \in \mathbb{R}$ is the control parameter that represents the normal acceleration. Note that $y(0) = 0$ and $x(0) > 0$ because the x axis is defined to point to the initial position of the interceptor.

In designing an optimal intercept guidance law, a common objective is to minimize the control effort of the interceptor. Thus, the free-time minimum-effort problem of the interceptor is usually solved to derive optimal intercept guidance law (see, e.g., Ref. [8]). We shall show by the following theorem that this problem is not a well-posed optimal control problem.

Theorem 1: Let $x_0 > 0$ and $\theta_0 \in [-\pi, \pi]$. Then, given any small $\varepsilon > 0$, there exists a time $t_f > 0$ and a control $u(\cdot)\colon [0, t_f] \to \mathbb{R}$ that steers (Σ) from $(x_0, 0)$ with the initial heading angle θ_0 to the origin $(0, 0)$ such that

$$\int_0^{t_f} \frac{1}{2} u^2(t)\,\mathrm{d}t < \varepsilon$$

The proof of this theorem is given in Appendix A.

Due to Theorem 1, a global solution for the free-time minimum-effort nonlinear optimal intercept problem does not exist. For this reason, we consider the following optimal intercept problem (OIP) for which the objective function is a linear combination of the control effort and engagement duration (see, e.g., Ref. [10]).

Problem 1 (OIP): Given $x_0 > 0$ and $\theta_0 \in [-\pi, \pi]$, the OIP consists of steering (Σ) by a measurable control $u(\cdot)$ on $[0, t_f]$ from the initial point $(x_0, 0)$ with the initial heading angle θ_0 to the final point $(0, 0)$ such that

$$J = \int_0^{t_f} \left[\kappa + \frac{1}{2}(1-\kappa)u^2(t)\right] \mathrm{d}t \tag{2}$$

is minimized where the final time $t_f > 0$ is free and $\kappa \in (0, 1)$ is a weighting factor.

If $\kappa = 1$, the OIP reduces to a minimum-time control problem, for which the optimal trajectory is a straight line because the control is not constrained; if $\kappa = 0$, no solution exists for the OIP, as shown by Theorem 1. By the following theorem, we shall show that, for every $\kappa \in (0, 1)$, the OIP has a global optimum.

Theorem 2: Given any $x_0 > 0$, $\theta_0 \in [-\pi, \pi]$, and $\kappa \in (0, 1)$, the OIP has a global optimum.

The proof of this theorem is given in Appendix B.

Before proceeding, we remark on the symmetric property of the solution of the OIP.

Remark 1: Given $x_0 > 0$ and $\theta_0 \in [-\pi, \pi]$, the optimal trajectory of the OIP with $[x(0), y(0), \theta(0)] = [x_0, 0, \theta_0]$ and that of the OIP with $[x(0), y(0), \theta(0)] = [x_0, 0, -\theta_0]$ are symmetric with respect to the x axis of frame Oxy. This indicates that the optimal trajectory of the OIP with the initial heading angle $\theta_0 \in (-\pi, 0)$ can be readily obtained by rotating the solution of the OIP with the initial heading angle $-\theta_0$. In addition, for any $x_0 > 0$, if the initial velocity vector points to the target [i.e., $\theta(0) = \pi$], the optimal trajectory of the OIP is a straight line, and hence the corresponding optimal control is zero. As a result, in the remainder of the paper, we will only consider that the initial heading angle θ_0 of the OIP is in $[0, \pi)$.

B. Necessary Conditions

Denote by p_x, p_y, and p_θ the costate variables of x, y, and θ, respectively. Then, the Hamiltonian for the OIP is expressed as

$$H = p_x \cos\theta + p_y \sin\theta + p_\theta u + p^0\left[\kappa + \frac{1}{2}(1-\kappa)u^2\right]$$

where p^0 is a nonpositive scalar.

According to Pontryagin's maximum principle [13], for $t \in [0, t_f]$, it holds that

$$\begin{cases} \dot{p}_x(t) = -\frac{\partial H}{\partial x} = 0, \\ \dot{p}_y(t) = -\frac{\partial H}{\partial y} = 0, \\ \dot{p}_\theta(t) = -\frac{\partial H}{\partial \theta} = p_x(t)\sin\theta(t) - p_y(t)\cos\theta(t) \end{cases} \tag{3}$$

and

$$\frac{\partial H}{\partial u} = 0 \tag{4}$$

Remark 2: When $p^0 = 0$, the explicit formula of Eq. (4) implies $p_\theta \equiv 0$, which indicates $\dot{p}_\theta \equiv 0$. According to the third equation of Eq. (3), if $\dot{p}_\theta \equiv 0$, the optimal trajectory of the OIP is a straight line, and hence the corresponding optimal control is null, which happens only if the initial velocity vector points to the target (or the initial heading angle θ_0 is π). Because p^0 is nonpositive, and because we consider the interval of θ_0 to be $[0, \pi)$ (see Remark 1), we have that p^0 is negative. For any negative p^0, the quadruple $(p_x, p_y, p_\theta, p^0)$ can be normalized so that $p^0 = -1$. Thus, we shall consider $p^0 = -1$ in the remainder of the paper.

As a result of this remark, explicitly rewriting Eq. (4) leads to

$$u(t) = \frac{1}{1-\kappa} p_\theta(t), \qquad t \in [0, t_f] \tag{5}$$

Because the final angle is free, the transversality condition implies

$$p_\theta(t_f) = 0 \tag{6}$$

As the final time is free, along the optimal trajectory, it holds

$$H \equiv 0 \tag{7}$$

In view of Eq. (3), we have that p_x and p_y are constants. Then, taking into account Eq. (6) and the final boundary condition $(x(t_f), y(t_f)) = (0, 0)$, we can integrate the third equation of Eq. (3) to yield

$$p_\theta(t) = p_x y(t) - p_y x(t), \qquad t \in [0, t_f] \tag{8}$$

Substituting Eq. (8) into Eq. (5), we obtain the optimal feedback control law:

$$u(t) = \frac{p_x y(t) - p_y x(t)}{1-\kappa}, \qquad t \in [0, t_f] \tag{9}$$

Note that the guidance law of PN [14] is expressed as

$$u(t) = NV\dot{\lambda}(t) \tag{10}$$

where V is the magnitude of the velocity $\boldsymbol{V}$ of the interceptor (normalized to one in this paper), N is the constant navigation gain, and $\dot{\lambda}$ is the LOS rate. According to the definition of the angle λ (see Fig. 1), we have

$$\tan[\lambda(t)] = \frac{y(t)}{x(t)}$$

Differentiating this equation with respect to time leads to the LOS rate as

$$\dot{\lambda}(t) = \frac{x(t)\sin\theta(t) - y(t)\cos\theta(t)}{x(t)^2 + y(t)^2}, \qquad t \in [0, t_f)$$

It should be noted that the LOS rate at the final time cannot be defined by this equation because $x(t_f)^2 + y(t_f)^2 = 0$. If $\dot{\lambda} \neq 0$, combining Eq. (9) with Eq. (10) leads to the optimal state-dependent navigation gain

$$N(t) = \frac{[p_x y(t) - p_y x(t)][x(t)^2 + y(t)^2]}{(1-\kappa)[x(t)\sin\theta(t) - y(t)\cos\theta(t)]}, \qquad t \in [0, t_f) \tag{11}$$

It is apparent from Eq. (11) that, in the nonlinear setting, the optimal navigation gain is not a constant any more.

The state variables $x(t)$ and $y(t)$ at each time $t \in [0, t_f]$ can be obtained by some sensors, e.g., inertial measurement unit (IMU). As a result, obtaining the optimal intercept guidance law of Eq. (9) or the optimal navigation gain of Eq. (11) amounts to computing the costate variables p_x and p_y. Generally, it is difficult to compute p_x and p_y because they are the solution of a two-point boundary value problem. In the subsequent sections, we shall present some geometric properties for the solution of the OIP and then use those properties to establish an efficient and robust method to compute p_x and p_y.

III. Characterizing the Solution of OIP

In this section, we first parameterize the aforementioned necessary conditions and then establish some properties for the solution of the OIP.

A. Parameterization

Define the constant $\alpha \geq 0$ as the norm of the vector $[p_x, p_y]$, i.e.,

$$\alpha := \sqrt{p_x^2 + p_y^2}$$

and set

$$\beta := n\pi + \tan^{-1}(-p_x/p_y) \tag{12}$$

where n is an integer. As a result, we have

$$p_x = \alpha \sin\beta \text{ and } p_y = -\alpha\cos\beta \tag{13}$$

Then, we can rewrite Eq. (8) as

$$p_\theta(t) = \alpha[x(t)\cos\beta + y(t)\sin\beta] \tag{14}$$

Substituting Eqs. (5) and (13) into the Hamiltonian and taking into account Eq. (7), we get

$$H(t) = \alpha\sin[\beta - \theta(t)] + \frac{1}{2(1-\kappa)} p_\theta^2(t) - \kappa = 0 \tag{15}$$

Evaluating Eq. (15) at $t = 0$ leads to

$$\alpha\sin(\beta - \theta_0) + \frac{\alpha^2}{2(1-\kappa)}(x_0\cos\beta)^2 = \kappa \tag{16}$$

Because $\alpha \geq 0$ and $\kappa \neq 0$, Eq. (16) implies $\alpha > 0$. Then, solving the quadratic equation in Eq. (16) indicates that α is a function of β, i.e.,

$$\alpha(\beta) = \begin{cases} \kappa/\sin(\beta - \theta_0), & \text{if } \cos\beta = 0 \text{ and } \sin(\beta-\theta_0) \neq 0, \\ (1-\kappa)\frac{-\sin(\beta-\theta_0) + \sqrt{\sin^2(\beta-\theta_0) + (2\kappa(x_0\cos\beta)^2/1-\kappa)}}{(x_0\cos\beta)^2} & \text{if } \cos\beta \neq 0 \end{cases}$$

As a result, by substituting Eq. (13) into Eq. (9), we eventually obtain that the optimal feedback control law is parameterized by the scalar β, i.e.,

$$u(t, \beta) = \frac{\alpha(\beta)}{1-\kappa}[x(t)\cos\beta + y(t)\sin\beta], \qquad t \in [0, t_f] \tag{17}$$

Thanks to Theorem 2, there exists at least one specific parameter β^* such that $u(t, \beta^*)$ for $t \in [0, t_f]$ is the optimal feedback control of the OIP. To this end, as the state variables $x(t)$ and $y(t)$ at each time can be obtained by some sensors (e.g., IMU), finding β^* is sufficient for deriving the optimal feedback control law in Eq. (17). In the next sections, we shall characterize the solution of the OIP so that the specific parameter β^* can be computed efficiently.

For notational simplicity, we denote hereafter by the triple $[x(t, \beta), y(t, \beta), \theta(t, \beta)]$ the integration of the differential equation (Σ)

from the initial condition $(x_0, 0, \theta_0)$ with the β-parameterized feedback control $u(t, \beta)$ in Eq. (17), i.e.,

$$\begin{bmatrix} x(t,\beta) \\ y(t,\beta) \\ \theta(t,\beta) \end{bmatrix} := \begin{bmatrix} x_0 \\ 0 \\ \theta_0 \end{bmatrix} + \int_0^t \begin{bmatrix} \cos\theta(\tau) \\ \sin\theta(\tau) \\ u(\tau,\beta) \end{bmatrix} \mathrm{d}\tau, \qquad t \geq 0$$

By the definition of β^*, it is clear that the triple $[x(t,\beta^*), y(t,\beta^*), \theta(t,\beta^*)]$ for $t \in [0, t_f]$ is the optimal trajectory of the OIP.

B. Properties of the OIP's Solution

In this subsection, some geometric properties for the solution of the OIP will be established by the following lemmas. For the simplicity of presentation, the proofs of all the lemmas are postponed to Appendix C.

Note that the space of β can be projected to any interval of length 2π [see the definition of β in Eq. (12)]. For later analyses, we consider that β lies in $[-\pi/2, 3\pi/2]$. By the following lemma, the interval of β can be further restricted.

Lemma 1: Given $x_0 > 0$, $\theta_0 \in [0, \pi]$ and $\kappa \in (0, 1)$, define the set

$$\mathcal{S} := \{\beta \in [-\pi/2, 3\pi/2]: \kappa(x_0\cos\beta)^2 - 2(1-\kappa)[\sin(\theta_0 - \beta) + 1] \leq 0\} \tag{18}$$

Then, we have $\beta^* \in \mathcal{S}$.

In the next lemma, we present an important property for p_θ, which will be used in the later analyses.

Lemma 2. Let $t_f > 0$ be the optimal final time of the OIP. For any $\beta^* \in \mathcal{S}$, such that $\alpha(\beta^*) \neq \kappa$, the following two statements hold:

1) If

$$\beta^* \in \mathcal{S} \cap (-\pi/2, \pi/2)$$

we have

$$p_\theta(t) = \alpha(\beta^*)[x(t,\beta^*)\cos\beta^* + y(t,\beta^*)\sin\beta^*] > 0$$

for $t \in (0, t_f)$.

2) If

$$\beta^* \in \mathcal{S} \cap (\pi/2, 3\pi/2)$$

we have

$$p_\theta(t) = \alpha(\beta^*)[x(t,\beta^*)\cos\beta^* + y(t,\beta^*)\sin\beta^*] < 0$$

for $t \in (0, t_f)$.

This lemma indicates that p_θ does not change its sign along the solution of the OIP. Combining this result with Eqs. (1) and (5) immediately leads to the following corollary:

Corollary 1: Let $t_f > 0$ be the optimal final time of the OIP. Then, the heading angle $\theta(t, \beta^*)$ for $t \in [0, t_f]$ monotonically increases (respectively, decreases) if $\beta^* \in (-\pi/2, \pi/2) \cap \mathcal{S}$ [respectively, $\beta^* \in (\pi/2, 3\pi/2) \cap \mathcal{S}$].

In the endgame stage of an engagement, it is common to keep the interceptor locked on to the target, which can be guaranteed by constraining the look angle σ (defined in Fig. 1) within $(-\pi/2, \pi/2)$. The following lemma presents some restriction of β^* for the fulfillment of $\sigma \in (-\pi/2, \pi/2)$ along the optimal trajectory of the OIP.

Lemma 3: Given any $x_0 > 0$ and any $\kappa \in (0, 1)$, if the look angle σ along the solution of the OIP is in $(-\pi/2, \pi/2)$, then $\theta_0 \in (\pi/2, \pi)$ and $\beta^* \in (-\pi/2, \pi/2) \cap \mathcal{S}$.

Let $\theta_f(\beta)$ be a function of $\beta \in \mathcal{S}$ such that Eq. (15) at $t = t_f$ is satisfied, i.e.,

$$H(t_f) = \alpha(\beta)\sin[\beta - \theta_f(\beta)] - \kappa = 0 \tag{19}$$

Notice that $\theta_f(\beta^*)$ is the optimal final heading angle of the OIP, i.e., $\theta(t_f, \beta^*) = \theta_f(\beta^*)$. In view of Eq. (15), we have

$$p_\theta(t) = \pm\sqrt{2(1-\kappa)}\sqrt{\kappa - \alpha(\beta)\sin(\beta - \theta(t))}$$

According to Lemma 2, this equation indicates

$$p_\theta(t) = \begin{cases} \sqrt{2(1-\kappa)}\sqrt{\kappa - \alpha(\beta)\sin(\beta - \theta(t))}, & \text{if } \beta \in (-\pi/2, \pi/2) \cap \mathcal{S} \\ -\sqrt{2(1-\kappa)}\sqrt{\kappa - \alpha(\beta)\sin(\beta - \theta(t))}, & \text{if } \beta \in (\pi/2, 3\pi/2) \cap \mathcal{S} \end{cases} \tag{20}$$

Combining Eq. (5) with $\dot{\theta} = u$ yields

$$\mathrm{d}t = (1-\kappa)\frac{\mathrm{d}\theta}{p_\theta} \tag{21}$$

Let $t_f(\beta)$ be the integration of Eq. (21) from θ_0 to $\theta_f(\beta)$, i.e.,

$$t_f(\beta) := (1-\kappa)\int_{\theta_0}^{\theta_f(\beta)} \frac{1}{p_\theta}\,\mathrm{d}\theta \tag{22}$$

Substituting Eqs. (20) and (22), we eventually have

$$t_f(\beta) = \begin{cases} \sqrt{\frac{1-\kappa}{2}}\int_{\theta_0}^{\theta_f(\beta)} \frac{1}{\sqrt{\kappa - \alpha(\beta)\sin(\beta-\theta)}}\,\mathrm{d}\theta, & \text{if } \beta \in (-\pi/2, \pi/2) \cap \mathcal{S} \\ \sqrt{\frac{1-\kappa}{2}}\int_{\theta_0}^{\theta_f(\beta)} \frac{-1}{\sqrt{\kappa - \alpha(\beta)\sin(\beta-\theta)}}\,\mathrm{d}\theta & \text{if } \beta \in (\pi/2, 3\pi/2) \cap \mathcal{S} \end{cases} \tag{23}$$

By the definition of β^*, we have that $t_f(\beta^*)$ is the optimal final time of the OIP. Because the target is located at the origin of frame Oxy, we have

$$(x(t_f(\beta^*), \beta^*), y(t_f(\beta^*), \beta^*)) = (0, 0)$$

To this end, one can find β^* by searching the common zeros of the two functions $x(t_f(\beta), \beta)$ and $y(t_f(\beta), \beta)$ over the interval $\mathcal{S}$. By the following lemma, we show that any zero of $y(t_f(\beta), \beta)$ is a zero of $x(t_f(\beta), \beta)$.

Lemma 4: Given any $\beta \in \mathcal{S}$, if $y(t_f(\beta), \beta) = 0$, then $x(t_f(\beta), \beta) = 0$.

As a result of this lemma, computing the common zeros of $x(t_f(\beta), \beta)$ and $y(t_f(\beta), \beta)$ is reduced to finding the zeros of the real-valued function $y(t_f(\beta), \beta)$ over the interval $\mathcal{S}$. In the next section, a semianalytical form for $y(t_f(\beta), \beta)$ will be derived so that a brute-force search method can be used to find its zero β^*.

IV. Semianalytical Solution

Combining Eqs. (1), (5), and (20) leads to

$$\sqrt{\frac{2}{1-\kappa}}\frac{\mathrm{d}y}{\mathrm{d}\theta} = \begin{cases} \frac{\sin\theta}{\sqrt{\kappa + \alpha(\beta)\sin(\theta - \beta)}}, & \text{if } \beta \in (-\pi/2, \pi/2) \cap \mathcal{S} \\ \frac{-\sin\theta}{\sqrt{\kappa + \alpha(\beta)\sin(\theta - \beta)}}, & \text{if } \beta \in (\pi/2, 3\pi/2) \cap \mathcal{S} \end{cases} \tag{24}$$

Taking into account $y(0) = 0$, we can integrate Eq. (24) to yield

$$\sqrt{\frac{2}{1-\kappa}}y(t_f(\beta), \beta) = \begin{cases} \int_{\theta_0}^{\theta_f(\beta)} \frac{\sin\theta}{\sqrt{\kappa + \alpha(\beta)\sin(\theta + \beta)}}\mathrm{d}\theta, & \text{if } \beta \in (-\pi/2, \pi/2) \cap \mathcal{S} \\ \int_{\theta_0}^{\theta_f(\beta)} \frac{-\sin\theta}{\sqrt{\kappa + \alpha(\beta)\sin(\theta + \beta)}}\mathrm{d}\theta, & \text{if } \beta \in (\pi/2, 3\pi/2) \cap \mathcal{S} \end{cases} \tag{25}$$

Rewriting Eq. (25) leads to

$$\sqrt{\frac{2}{1-\kappa}}y(t_f(\beta),\beta) = \begin{cases} \int_{\psi_0}^{\psi_f} \frac{\sin\beta\cos\psi}{\sqrt{\kappa+\alpha(\beta)\sin\psi}}\mathrm{d}\psi + \int_{\psi_0}^{\psi_f} \frac{\cos\beta\sin\psi}{\sqrt{\kappa+\alpha(\beta)\sin\psi}}\,\mathrm{d}\psi, & \text{if } \beta\in(-\pi/2,\pi/2)\cap\mathcal{S} \\ \int_{\psi_0}^{\psi_f} \frac{-\sin\beta\cos\psi}{\sqrt{\kappa+\alpha(\beta)\sin\psi}}\mathrm{d}\psi + \int_{\psi_0}^{\psi_f} \frac{-\cos\beta\sin\psi}{\sqrt{\kappa+\alpha(\beta)\sin\psi}}\,\mathrm{d}\psi, & \text{if } \beta\in(\pi/2,3\pi/2)\cap\mathcal{S} \end{cases} \tag{26}$$

where $\psi = \theta - \beta$, $\psi_0 = \theta_0 - \beta$, and $\psi_f = \theta_f(\beta) - \beta$. Note that we have

$$\begin{aligned}\int_{\psi_0}^{\psi_f} \frac{\cos(\psi)}{\sqrt{\kappa+\alpha(\beta)\sin(\psi)}}\,\mathrm{d}\psi &= \int_{\sin\psi_0}^{\sin\psi_f} \frac{1}{\sqrt{\kappa+\alpha(\beta)\sin(\psi)}}\,\mathrm{d}\sin\psi \\ &= \frac{2}{\alpha(\beta)}\sqrt{\kappa+\alpha(\beta)\sin\psi}\Big|_{\psi_0}^{\psi_f} \\ &= \frac{2}{\alpha(\beta)}\sqrt{\kappa-\alpha(\beta)\sin(\beta-\theta)}\Big|_{\theta_0}^{\theta_f(\beta)} \\ &= -\frac{2}{\alpha(\beta)}\sqrt{\kappa-\alpha(\beta)\sin(\beta-\theta_0)}\end{aligned} \tag{27}$$

where the final equality holds because of Eqs. (6) and (20). We also have

$$\begin{aligned}&\int_{\psi_0}^{\psi_f} \frac{\sin(\psi)}{\sqrt{\kappa+\alpha(\beta)\sin(\psi)}}\,\mathrm{d}\psi \\ &= \int_{\psi_0}^{\psi_f} \frac{\sqrt{\kappa+\alpha(\beta)\sin(\psi)}}{\alpha(\beta)}\,\mathrm{d}\psi + \int_{\psi_0}^{\psi_f} \frac{-\kappa/\alpha(\beta)}{\sqrt{\kappa+\alpha(\beta)\sin(\psi)}}\,\mathrm{d}\psi \\ &= \frac{\sqrt{\kappa+\alpha(\beta)}}{\alpha(\beta)}\int_{\psi_0}^{\psi_f}\sqrt{1-\frac{2\alpha(\beta)}{\kappa+\alpha(\beta)}\sin^2(\psi/2-\pi/4)}\,\mathrm{d}\psi \\ &- \frac{\kappa}{\alpha(\beta)\sqrt{\kappa+\alpha(\beta)}}\int_{\psi_0}^{\psi_f} 1\Big/\sqrt{1-\frac{2\alpha(\beta)}{\kappa+\alpha(\beta)}\sin^2(\psi/2-\pi/4)}\,\mathrm{d}\psi \\ &= -\frac{2\sqrt{\kappa+\alpha(\beta)}}{\alpha(\beta)}E\left[\frac{\pi}{4}-\frac{\psi}{2},\frac{2\alpha(\beta)}{\kappa+\alpha(\beta)}\right]\Big|_{\psi_0}^{\psi_f} \\ &+ \frac{2\kappa}{\alpha(\beta)\sqrt{\kappa+\alpha(\beta)}}F\left[\frac{\pi}{4}-\frac{\psi}{2},\frac{2\alpha(\beta)}{\kappa+\alpha(\beta)}\right]\Big|_{\psi_0}^{\psi_f}\end{aligned} \tag{28}$$

where $F(\cdot,\cdot)$ and $E(\cdot,\cdot)$ are the incomplete elliptic integrals of the first and second kinds, respectively (see, e.g., Ref. [15] for details of the two elliptic integrals). Substituting Eqs. (27) and (28) into Eq. (26) eventually yields

$$\begin{aligned}y(t_f(\beta),\beta) = &\left\{\frac{2\sin\beta}{\alpha(\beta)}\sqrt{\kappa+\alpha(\beta)\sin\psi_0}\right. \\ &-\frac{2\cos\beta\sqrt{\kappa+\alpha(\beta)}}{\alpha(\beta)}\left[E\left(\frac{\pi}{4}-\frac{\psi_0}{2},\frac{2\alpha(\beta)}{\kappa+\alpha(\beta)}\right)-E\left(\frac{\pi}{4}-\frac{\psi_f}{2},\frac{2\alpha(\beta)}{\kappa+\alpha(\beta)}\right)\right] \\ &\left.+\frac{2\kappa\cos\beta}{\alpha(\beta)\sqrt{\kappa+\alpha(\beta)}}\left[F\left(\frac{\pi}{4}-\frac{\psi_0}{2},\frac{2\alpha(\beta)}{\kappa+\alpha(\beta)}\right)-F\left(\frac{\pi}{4}-\frac{\psi_f}{2},\frac{2\alpha(\beta)}{\kappa+\alpha(\beta)}\right)\right]\right\} \\ &\times\sqrt{\frac{1-\kappa}{2}},\quad \text{if } \beta\in(-\pi/2,\pi/2)\cap\mathcal{S}\end{aligned} \tag{29}$$

$$\begin{aligned}y(t_f(\beta),\beta) = -&\left\{\frac{2\sin\beta}{\alpha(\beta)}\sqrt{\kappa+\alpha(\beta)\sin\psi_0}\right. \\ &-\frac{2\cos\beta\sqrt{\kappa+\alpha(\beta)}}{\alpha(\beta)}\left[E\left(\frac{\pi}{4}-\frac{\psi_0}{2},\frac{2\alpha(\beta)}{\kappa+\alpha(\beta)}\right)-E\left(\frac{\pi}{4}-\frac{\psi_f}{2},\frac{2\alpha(\beta)}{\kappa+\alpha(\beta)}\right)\right] \\ &\left.+\frac{2\kappa\cos\beta}{\alpha(\beta)\sqrt{\kappa+\alpha(\beta)}}\left[F\left(\frac{\pi}{4}-\frac{\psi_0}{2},\frac{2\alpha(\beta)}{\kappa+\alpha(\beta)}\right)-F\left(\frac{\pi}{4}-\frac{\psi_f}{2},\frac{2\alpha(\beta)}{\kappa+\alpha(\beta)}\right)\right]\right\} \\ &\times\sqrt{\frac{1-\kappa}{2}},\quad \text{if } \beta\in(\pi/2,3\pi/2)\cap\mathcal{S}\end{aligned} \tag{30}$$

Given any $\beta\in\mathcal{S}$, the value of $y(t_f(\beta),\beta)$ in either Eq. (29) or Eq. (30) can be immediately obtained because the elliptic integrals $E(\cdot,\cdot)$ and $F(\cdot,\cdot)$ have series representations like the simple sine and cosine functions.

As a result, a brute-force search method can be used to find the zero β^* of $y(t_f(\beta),\beta)$ over the two intervals $(-\pi/2,\pi/2)\cap\mathcal{S}$ and $(\pi/2,3\pi/2)\cap\mathcal{S}$ if the boundaries of $\mathcal{S}$ are available. By the following lemma, the boundaries of the set $\mathcal{S}$ will be presented.

Lemma 5: Given $x_0 > 0$ and $\theta_0\in[0,\pi)$, let

$$M = \min_{\beta\in(-\pi/2,\pi/2)}\left\{\frac{2[\sin(\theta_0-\beta)+1]}{x_0^2\cos^2\beta + 2[\sin(\theta_0-\beta)+1]}\right\} \tag{31}$$

We have that $M > 0$, and the following statements hold:

1) If $\kappa\le M$, we have $(-\pi/2,\pi/2)\cap\mathcal{S} = (-\pi/2,\pi/2)$.

2) If $\kappa > M$, there exists β_1 and β_2 in $(-\pi/2,\pi/2)$ with $\beta_1 < \beta_2$ such that

$$(-\pi/2,\pi/2)\cap\mathcal{S} = (-\pi/2,\beta_1)\cup(\beta_2,\pi/2)$$

and $\tan(\beta_1/2)$ and $\tan(\beta_2/2)$ are two different zeros of the following fourth-degree polynomial in terms of x:

$$\begin{aligned}0 = &[\kappa x_0^2 - 2(1-\kappa)(1-\sin\theta_0)]x^4 + 4(1-\kappa)\cos\theta_0 x^3 \\ &- 2[\kappa x_0^2 + 2(1-\kappa)]x^2 + 4(1-\kappa)\cos\theta_0 x + \kappa x_0^2 - 2(1-\kappa)\end{aligned} \tag{32}$$

3) In any case, there exist β_3 and β_4 in $(\pi/2,3\pi/2)$ with $\beta_3 < \beta_4$ such that

$$(\pi/2,3\pi/2)\cap\mathcal{S} = (\pi/2,\beta_3)\cup(\beta_4,3\pi/2)$$

and $\tan(\beta_3/2)$ and $\tan(\beta_4/2)$ are two different zeros of the polynomial in Eq. (32).

The proof of this lemma is postponed to Appendix C. Lemma 5 indicates that the zero β^* of $y(t_f(\beta),\beta)$ must lie in three or four shorter intervals, depending on the relationship between κ and M in Eq. (31). Note that a fourth-degree polynomial can be solved either in an analytical way or by using a standard polynomial solver. Thus, the boundaries $\beta_1,\ldots,\beta_4$ (if they exist) of the three or four shorter intervals can be readily computed by solving the fourth-degree polynomial in Eq. (32). Also notice that the function $y(t_f(\beta),\beta)$ is continuous on the three or four shorter intervals. As a result, a brute-force search method can be used to find the zero β^* of $y(t_f(\beta),\beta)$ on each interval if it exists, as shown by Algorithm 1.

Let us gather a few words to explain the brute-force search method in Algorithm 1. If the discretization level $l\in\mathbb{N}$ is large enough, the method can find all the zeros of $y(t_f(\beta),\beta)$ within the three or four intervals established in Lemma 5. Note that we have devised a semianalytical form for $y(t_f(\beta),\beta)$ so that its value can be efficiently computed for every $\beta\in\mathcal{S}$ [cf. Eqs. (29) and (30)]. Therefore, the brute-force search method is in fact not time consuming, as demonstrated by the numerical simulations in the next section.

V. Numerical Simulations

In the following three subsections, we present three numerical cases (A, B, and C) to demonstrate the developments of the paper and to examine the viability of the developed nonlinear optimal guidance law.

Algorithm 1 Brute-force search for finding β^*

	Given $x_0 > 0$, $\theta_0 \in [0, \pi)$, and $\kappa \in (0, 1)$, the brute-force search method is performed as follows:
Step 1:	Let $l \in \mathbb{N}$ be a positive integer.
Step 2:	Let (b_1, b_2) be one of the three or four continuous intervals established in Lemma 5.
Step 3	Let $\beta(j) = b_1 + j \times (b_2 - b_1)/l$ for $j = 0, \ldots, l$ and set $i = 1$.
Step 4:	If $i \leq l$, go to step 4.1; otherwise, go to end;
Step 4.1:	If $y(t_f(\beta(i-1)), \beta(i-1)) \times y(t_f(\beta(i)), \beta(i)) < 0$, use a bisection method to find β^* between $\beta(i-1)$ and $\beta(i)$;
Step 4.2:	Set $i = i + 1$ and go back to step 4.
Step 5:	End.

Table 1 Case A: values of β^* and $t_f(\beta^*)$ of the two local solutions for $\kappa = 10^{-1}, \ldots, 10^{-10}$

	Data associated with β_1^*		Data associated with β_2^*	
κ	β_1^*	$t_f(\beta_1^*)$	β_2^*	$t_f(\beta_2^*)$
10^{-1}	4.7166	1.0018×10^3	4.7082	1.0102×10^3
10^{-2}	4.7266	1.0058×10^3	4.6984	1.0340×10^3
10^{-3}	4.7581	1.0185×10^3	4.6687	1.1079×10^3
10^{-4}	4.8647	1.0582×10^3	4.5802	1.3417×10^3
10^{-5}	5.3000	1.1685×10^3	4.3462	2.0876×10^3
10^{-6}	0.4608	1.3238×10^3	3.9612	4.5731×10^4
10^{-7}	0.8744	1.3942×10^3	3.8882	1.2799×10^3
10^{-8}	0.9184	1.4056×10^3	3.9536	3.8566×10^4
10^{-9}	0.9229	1.4069×10^3	3.9855	1.1969×10^5
10^{-10}	0.9233	1.4070×10^3	3.9966	3.7605×10^5

A. Selection of the Value of κ in (0,1)

For case A, we will demonstrate the solutions of the OIP (Problem 1) for different $\kappa \in [10^{-10}, 10^{-1}]$ but with fixed initial conditions: $x_0 = 1000$ m and $\theta_0 = \pi/2$. Notice that $y_0 = 0$ as the x axis points to the initial position of the interceptor, and that the magnitude of velocity has been normalized to one, i.e., $\|V\| = 1$ m/s. Using the brute-force search method in Algorithm 1, two zeros of $y(t_f(\beta), \beta)$ are found for each κ, indicating that, for each OIP, there exist two candidate solutions satisfying all the necessary conditions given in Sec. II. In fact, for each $\kappa \in [10^{-10}, 10^{-1}]$, one zero of $y(t_f(\beta), \beta)$ lies in $(-\pi/2, \pi/2)$ and another zero lies in $(\pi/2, 3\pi/2)$. For notational simplicity, we denote by β_1^* and β_2^* the zeros of $y(t_f(\beta), \beta)$ in $(-\pi/2, \pi/2)$ and $(\pi/2, 3\pi/2)$, respectively. Table 1 presents the values of β^* and $t_f(\beta^*)$ for the two local solutions of case A with $\kappa = 10^{-1}, \ldots, 10^{-10}$, and Fig. 2 shows the local optimal trajectories corresponding to the data in Table 1. It is interesting to notice from Table 1 and Fig. 2 that, although the candidate trajectories with $\beta^* \in (-\pi/2, \pi/2)$ are almost identical for $\kappa \leq 10^{-8}$, the trajectories associated with $\beta^* \in (\pi/2, 3\pi/2)$ become longer and longer as κ decreases.

The profiles of control as a function of time along the candidate solutions of the OIP for $\kappa = 10^{-10}, \ldots, 10^{-1}$ are plotted in Fig. 3, where the engagement durations are normalized to one for comparison purposes. It is seen from Fig. 3 that, the smaller κ is, the smaller the absolute value of control tends to be.

Once the solution of the OIP is computed for $\kappa \in (0, 1)$, we are able to compute the cost in Eq. (2), the control effort, and the engagement duration, as shown in Fig. 4 for different $\kappa \in [10^{-10}, 10^{-1}]$ with a log scale.

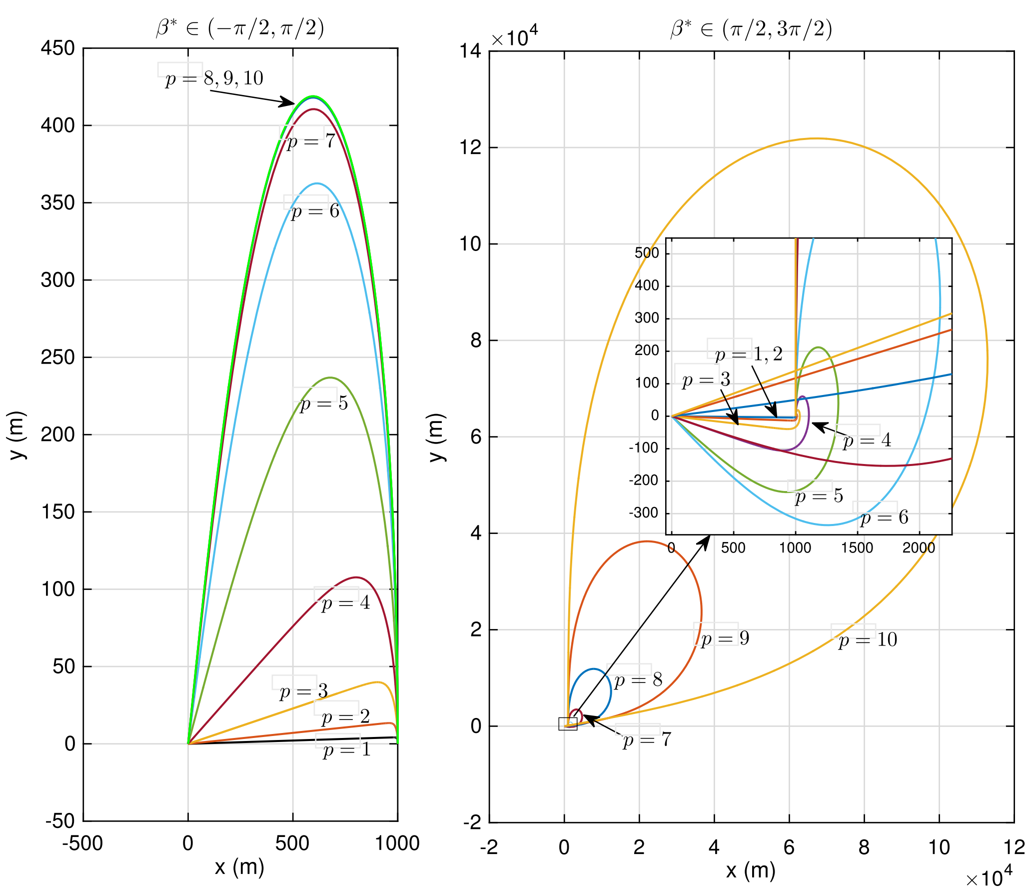

Fig. 2 Case A: Candidate trajectories for $\kappa = 10^{-p}$ with $p = 1, \ldots, 10$.

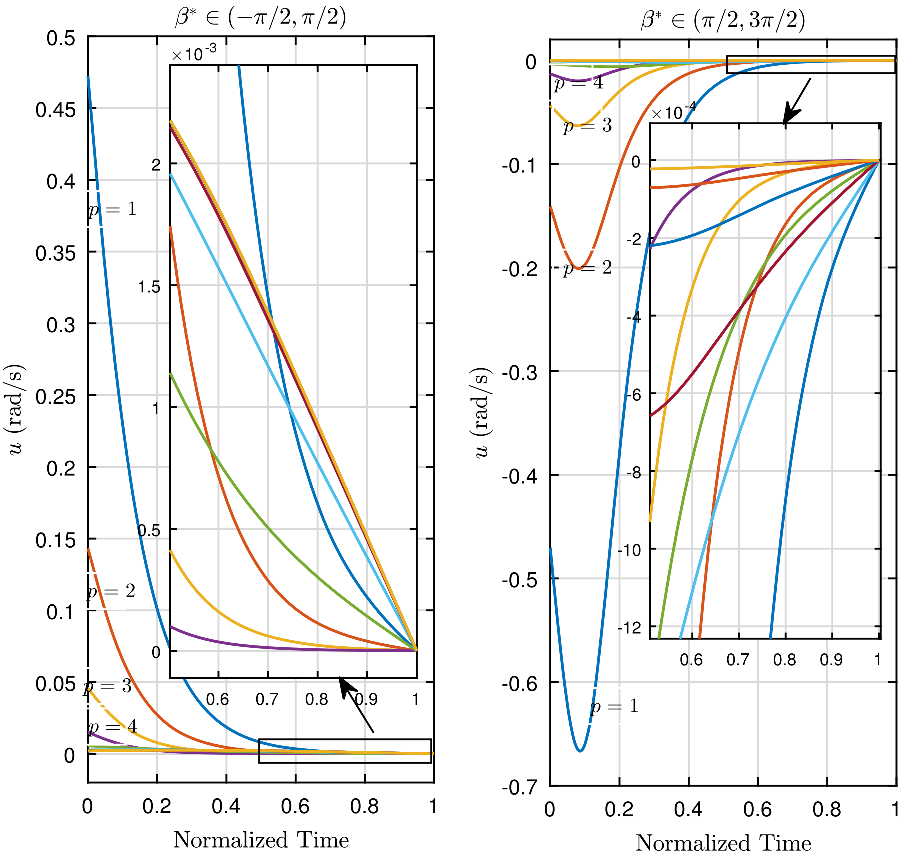

Fig. 3 Case A: The profiles of control along the optimal trajectories of the OIP for $\kappa = 10^{-p}$ with $p = 1, \ldots, 10$.

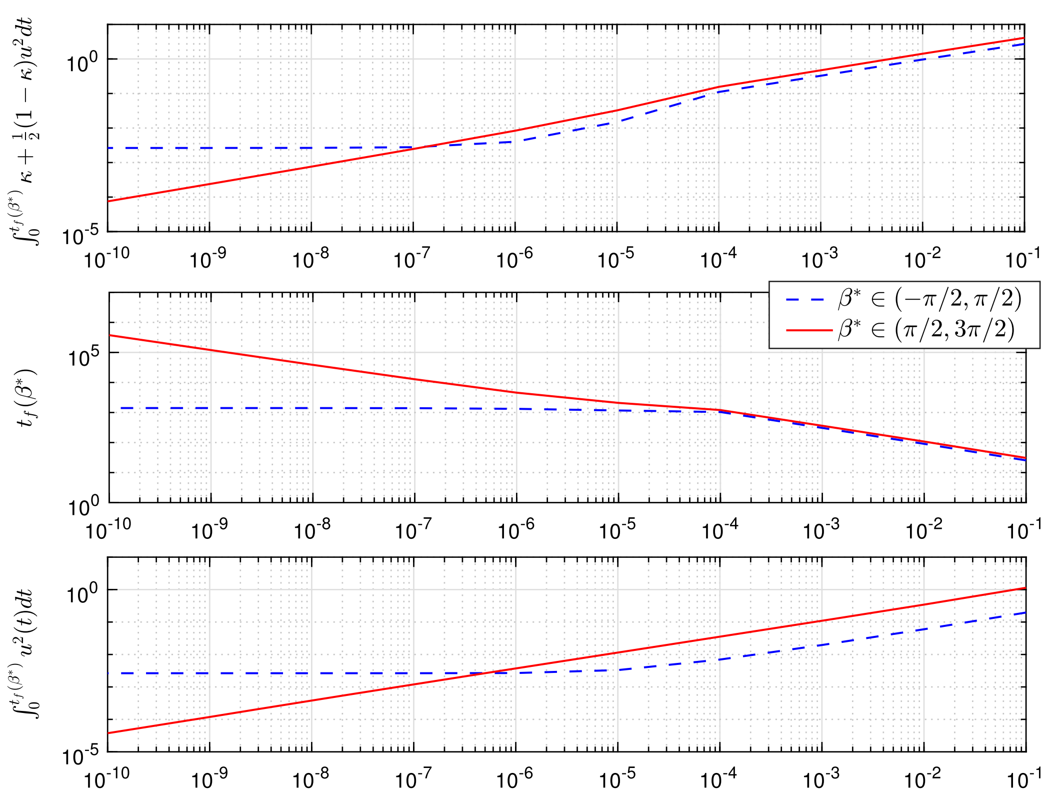

Fig. 4 Case A: The cost $J = \int_0^{t_f(\beta^*)} \kappa + (1/2)(1-\kappa)u^2(t)\,dt$, the control effort $\int_0^{t_f(\beta^*)} u^2(t)\,dt$, and the final time $t_f(\beta^*)$ against κ on $[10^{-1}, 10^{-10}]$.

We can see from Fig. 4 that the cost in Eq. (2) and the control effort of the two local solutions are monotonically decreasing with the decrease of κ. From the top graph of Fig. 4, it is seen that, for κ larger than around 10^{-7}, the performances of the shorter candidates associated with $\beta^* \in (-\pi/2, \pi/2)$ are better than those of the longer candidates; whereas the longer candidates associated with $\beta^* \in (\pi/2, 3\pi/2)$ have better performances for κ smaller than around 10^{-7}. We can see from the middle graph of Fig. 4 that the final time is monotonically nondecreasing with the decrease of κ from 10^{-1} to 10^{-10}. Actually, the trends of the two solid curves of the final time and the control effort in Fig. 4 coincide with Theorem 1. We can also see from Fig. 4 that, if κ is in between 10^{-1} and around 10^{-6}, the control efforts of the shorter candidates associated with $\beta^* \in (-\pi/2, \pi/2)$ are smaller than those of the longer candidates associated with $\beta^* \in (\pi/2, 3\pi/2)$; in addition, the control efforts and final times for the shorter candidates associated with $\beta^* \in (-\pi/2, \pi/2)$ almost do not change for κ larger than 10^{-6}. Therefore, in order to apply the nonlinear optimal guidance law, one should appropriately select $\kappa \in (0, 1)$ to balance between the engagement duration and the control effort.

B. Solution of the OIP with a Fixed κ

In this subsection, we shall present an example (case B) with a fixed κ to demonstrate the properties established in Sec. III. We set $\kappa = 10^{-5}$ and choose $x_0 = 10$ m and $\theta_0 = \pi/2$. By employing the brute-force search method in Algorithm 1 again, two zeros (i.e., $\beta_1^* = 0.9229$ and $\beta_2^* = 3.9855$) of $y(t_f(\beta), \beta)$ are found, indicating that there are two candidate trajectories satisfying all the necessary conditions given in Sec. II. The final times for the two candidates are $t_f(\beta_1^*) = 14.07$ s and $t_f(\beta_2^*) = 1196.86$ s.

By coding the brute-force search method in MATLAB, finding each zero of $y(t_f(\beta), \beta)$ for case B takes about 0.215 s on a desktop with an Intel® Core™ i7-3615QM CPU with 2.30 GHz. It is worth mentioning that the successive optimization method in Ref. [12] can converge to a local solution in the same scale of computer time. However, there may exist multiple local solutions for an OIP (for case B, there indeed exist two local solutions). In this case, the method in Ref. [12] is not able to guarantee the found solution to be the global optimal one. Thanks to the developments in the paper, all local solutions can be found efficiently, and we can choose one local solution according to mission requirements.

The two candidate trajectories are plotted in Fig. 5. Because β_1^* and β_2^* lie in $(-\pi/2, \pi/2)$ and $(\pi/2, 3\pi/2)$, respectively, it follows from Corollary 1 that the heading angle θ is monotonically increasing and decreasing along the shorter and longer trajectories, respectively, as shown in Fig. 6.

The profiles of control along the two candidate trajectories are plotted in Fig. 7, from which it is seen that the control is positive along the shorter candidate but it is negative along the longer candidate.

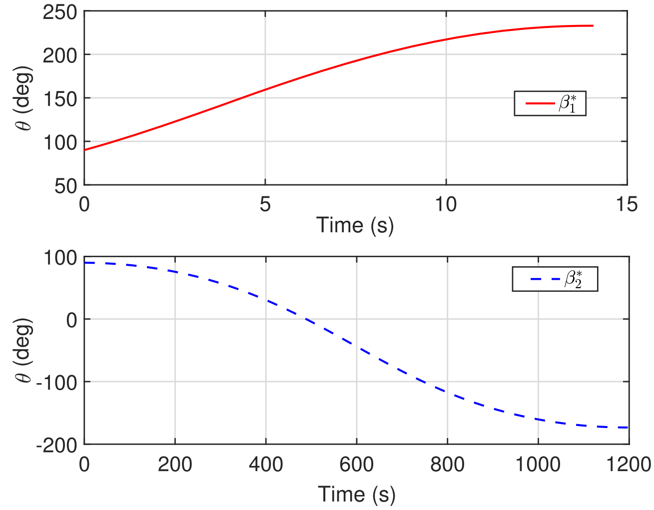

Fig. 6 Case B: Profiles of the heading angle θ along the shorter and the longer candidate trajectories.

The look angles σ along the two candidate trajectories are presented in Fig. 8. It is seen from Fig. 8 that the look angle along the shorter candidate trajectory associated with β_1^* is no more than 90 deg, as predicted by Lemma 3. If having the look angle in $[-\pi/2, \pi/2]$ is a primary constraint, one should choose the control law along the shorter candidate trajectory.

The profiles of the optimal state-dependent navigation gain $N(t)$ in Eq. (11) along the two candidate trajectories are plotted in Fig. 9. Note that, in each subfigure of Fig. 9, the navigation gain $N(t)$ is plotted to a time slightly earlier than the final time because the navigation gain is not defined at the final time [see Eq. (11)]. From Fig. 9, we can see that the optimal navigation gain along the longer candidate trajectory is negative until it goes to infinity around $t = 133.26$ s; after which, the optimal navigation gain is positive and it converges to three. In fact, the occurrence of negative navigation gain

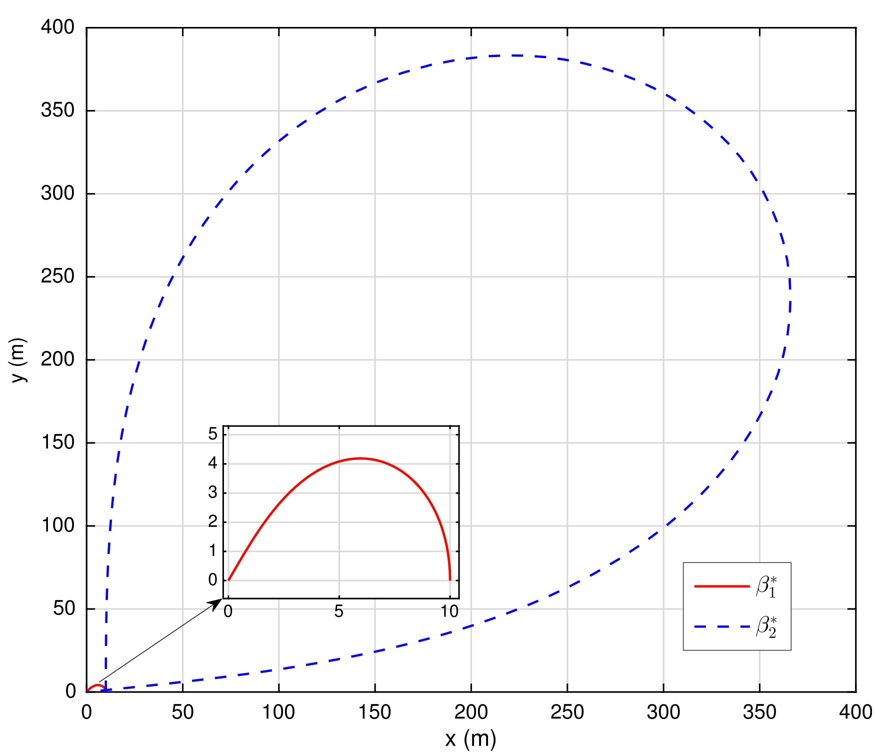

Fig. 5 Case B: The two candidate trajectories of the OIP (the subplot is scaled for the shorter path).

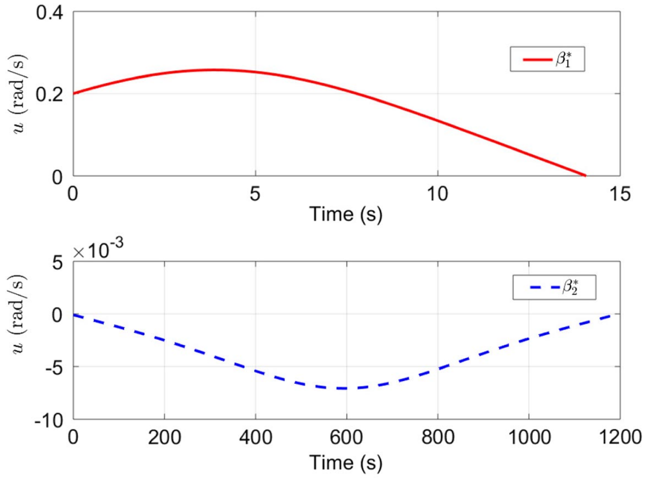

Fig. 7 Case B: The profiles of the control along the shorter and the longer candidate trajectories.

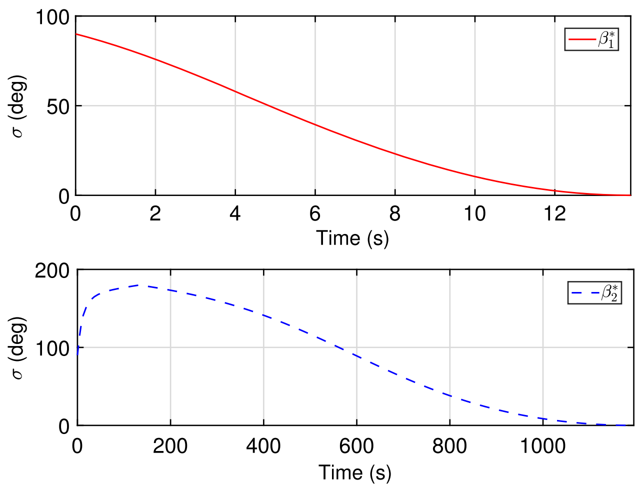

Fig. 8 Case B: Profiles of the look angles σ along the shorter and the longer candidate trajectories.

is due to the fact that the interceptor moves away from the target initially (see the longer candidate in Fig. 5). We can see from Fig. 9 that the optimal navigation gain $N(t)$ along the shorter candidate trajectory takes values between two and three, and it converges to three finally. Notice that, along both candidate trajectories, as the interceptor approaches the target, its trajectory converges to a straight line (see Fig. 5). In this part of the trajectory, there are small deviations around this line making linearization valid, and thus the gain converges to three, which is identical to the gain of the classical PN derived from the linearized case.

For comparison, the candidate trajectory associated with β_1^* as well as the trajectories generated by PN with $N = 2, \ldots, 5$ are plotted in Fig. 10. It is seen from Fig. 10 that the candidate trajectory associated with β_1^* is not the same as the trajectory generated by PN with $N = 3$, although PN with $N = 3$ is considered to be the optimal guidance law [6,7] (derived, as discussed earlier, under linearization assumptions). The control efforts along the trajectories generated by PN with $N = 2, \ldots, 5$ and along the optimal trajectories for β_1^* and β_2^* are numerically computed and presented in Table 2.

It is clear that the control effort along the longer candidate trajectory associated with β_2^* is the smallest. However, the longer candidate trajectory cannot be generated by the classical PN with a positive navigation gain because the navigation gain along the longer candidate trajectory can be negative (see Fig. 9). Notice from Table 2 that the shorter candidate has a control effort close to that obtained for PN with $N = 3$, indicating that, for case B, if we wish to minimize only the control effort, then PN with $N = 3$ serves almost as the optimal guidance law. In the next subsection, an example with a relatively large initial heading error will be presented to compare the nonlinear optimal guidance law with PN.

C. The Solution of OIP with $\|\sigma_0\|$ Greater Than $\pi/2$

For case C, we consider that $x_0 = 10$ and $\theta_0 = \pi/4$. This initial heading angle θ_0 indicates that the initial look angle is $\sigma_0 = 3\pi/4$. Even if the initial look angle σ_0 is not in $[-\pi/2, \pi/2]$, we can still employ PN to guide the pursuer of Eq. (1) from the given initial condition to the target (the origin of frame Oxy in Fig. 1), as shown by the trajectories generated by PN with feasible navigation gains in Fig. 11.

Table 3 presents the engagement duration and control effort of every trajectory in Fig. 11. It is clear from Table 3 that, for case C, if

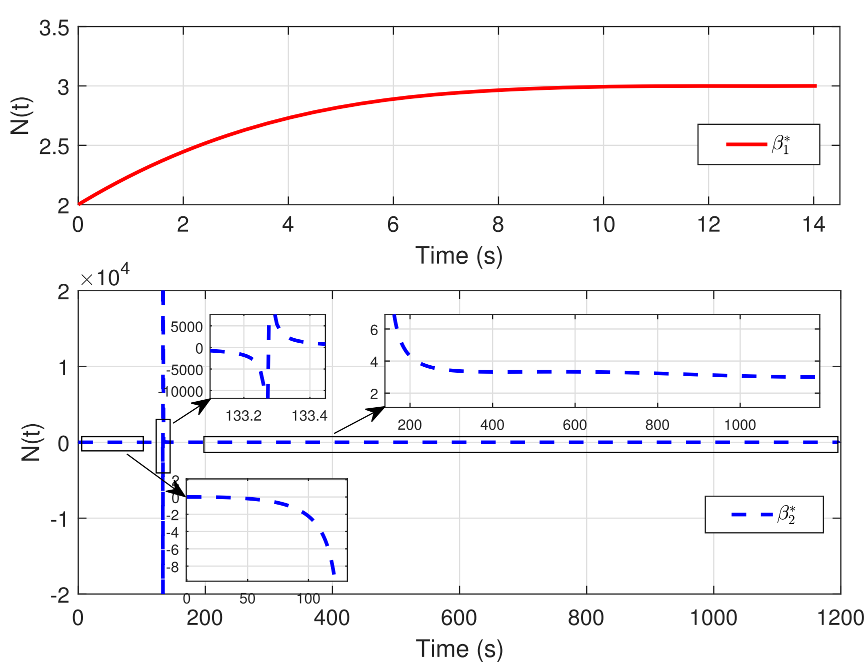

Fig. 9 Case B: Profiles of the optimal state-dependent navigation gain in Eq. (11) against time along the shorter and the longer candidate trajectories.

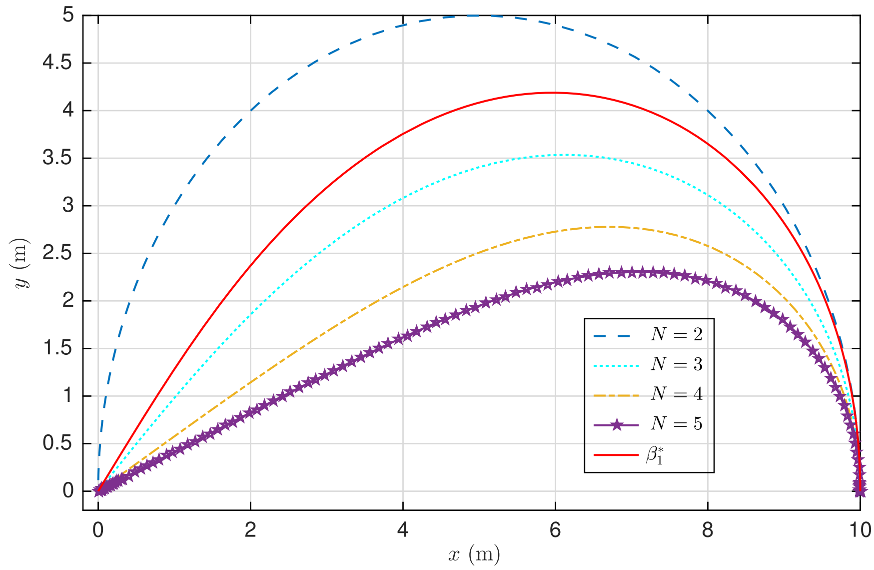

Fig. 10 Case B: Candidate trajectory with β_1^* and the trajectories generated by PN with $N = 2, \ldots, 5$.

we wish to minimize only the control effort, then the best navigation gain for PN is around two instead of being three.

To compare the nonlinear optimal guidance law with PN, the solution of case C is computed for different $\kappa \in (0, 1)$ by the brute-force search using Algorithm 1, and the optimal trajectories for some selected κ are plotted in Fig. 12. The engagement duration and control effort for every trajectory in Fig. 12 are listed in Table 4. Although the engagement duration of the shorter candidate trajectory with $\kappa = 0.005$ is close to the engagement duration of PN with the best navigation gain of $N = 2$ (compare Tables 3 and 4), the control effort of the shorter candidate is just 0.2725, which is around 80% of the control effort (0.3332) using PN with $N = 2$. We can see from Table 3 that the control effort of using PN is not monotonically decreasing with the increase of the engagement duration. However, the control effort of the optimal guidance law is monotonically decreasing with the increase of engagement duration according to Table 4. Therefore, in order to apply the nonlinear optimal guidance law of the paper, we should appropriately select $\kappa \in (0, 1)$ to balance the engagement duration and the control effort.

It is interesting to notice that all the numerical examples presented have two candidate solutions [the function $y(t_f(\beta), \beta)$ has two zeros for all of the aforementioned examples). In fact, a large number of additional simulations with different values of x_0, θ_0, and κ were carried out, showing that the function $y(t_f(\beta), \beta)$ always has two zeros for each example, and that the two zeros always lie in two different subintervals $(-\pi/2, \pi/2)$ and $(\pi/2, 3\pi/2)$. Although we are not able to provide rigorous proof for this interesting numerical result in this paper, the brute-force search method in Algorithm 1 can find all of them if the discretization level l is large enough.

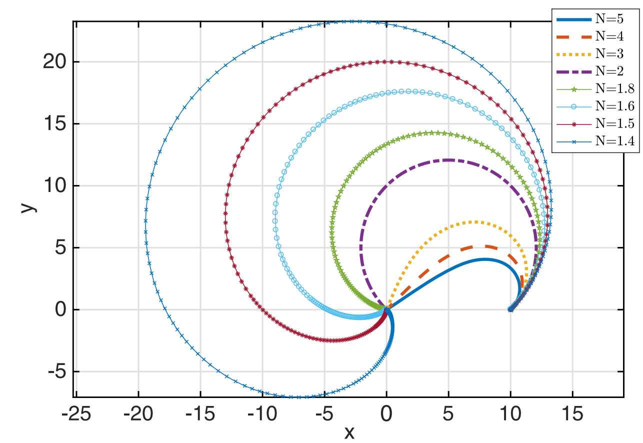

Fig. 11 Case C: Profiles of the trajectories generated by PN with different navigation gains.

VI. Conclusions

In this paper, it was first shown that a global solution does not exist for the typical free-time minimum-effort nonlinear optimal control problem of intercepting a stationary target. Thus, an optimal intercept problem, for which the objective function is a linear combination of control effort and engagement duration, was studied instead. By parameterizing the necessary conditions for optimality, it was found that the optimal guidance law is determined by the zeros of a real-valued function. As a semianalytical form for the real-valued function was devised, a simple brute-force search could be used to find all the zeros. Numerical simulations showed that, for each example, the corresponding real-valued function had two zeros, indicating that each example had two candidate trajectories. Between the two candidate trajectories, the heading angle monotonically increased along the shorter candidate, but it monotonically decreased along the longer candidate. If the weighting factor on engagement duration was relatively large, the shorter candidate consumed less control effort than the longer candidate; whereas, if it was relatively small, the longer candidate would consume less control effort. Thus, in order to apply the nonlinear optimal guidance law, $\kappa \in (0, 1)$ should be appropriately selected to balance between the engagement duration and the control effort; and for realistic engagements with tight timing

Table 2 Case B: control effort of trajectories generated by PN and two local optimal trajectories

	Parameter					
	N				β^*	
Performance	2	3	4	5	β_1^*	β_2^*
Engagement duration, s	15.7080	13.1103	12.1433	11.6359	14.0686	1196.86
Control effort $\int_0^{t_f} (1/2)u^2(t)\,\mathrm{d}t$	0.3142	0.2697	0.2989	0.3396	0.2646	0.0119

Table 3 Case C: engagement duration and control effort of the trajectories generated by PN with different navigation gains

N	1.4	1.5	1.6	1.8	2	3	4	5
t_f	92.0081	68.2842	54.9906	40.7584	33.3216	20.5314	16.7999	15.0213
$\int_0^{t_f}(1/2)u^2(t)\,\mathrm{d}t$	100.7859	1.9369	0.5371	0.3592	0.3332	0.3675	0.4399	0.5191

Table 4 Case C: engagement duration and control effort of the optimal trajectories with various κ

	Data associated with β_1^*		Data associated with β_2^*	
κ	$t_f(\beta_1^*)$	$\int_0^{t_f(\beta_1^*)}(1/2)u^2(t,\beta_1^*)\,\mathrm{d}t$	$t_f(\beta_2^*)$	$\int_0^{t_f(\beta_2^*)}(1/2)u^2(t,\beta_2^*)\,\mathrm{d}t$
1×10^{-2}	22.0973	0.3492	40.0366	0.3658
8×10^{-3}	24.4196	0.3283	44.0946	0.3292
5×10^{-3}	33.3705	0.2725	54.5506	0.2627
4×10^{-3}	39.8225	0.2435	60.5668	0.2356
3×10^{-3}	49.5712	0.2096	69.4870	0.2046
2×10^{-3}	65.7617	0.1699	84.6234	0.1675
1×10^{-3}	101.4470	0.1193	119.1560	0.1186

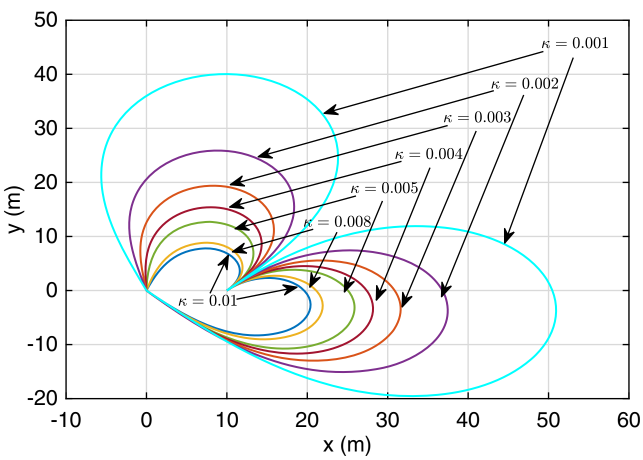

Fig. 12 Case C: Profiles of the optimal trajectories with different κ.

constraints, it is expected that the shorter candidate optimal solution will be used.

Appendix A: Proof of Theorem 1

Given any points z_0 and z_f in $\mathbb{R}^2$, let θ_0 and θ_f in $[0, 2\pi]$ be the heading angles at z_0 and z_f, respectively. Then, there always exists a path concatenating by a circular arc and two straight lines so that the initial point z_0 with the heading angle θ_0 and the final point z_f with the heading angle θ_f are connected by the path, as shown in Fig. A1. Let $u_c > 0$ be the control along the circular arc. It is clear that $u_c = 1/\rho$ is a constant where $\rho > 0$ is the radius of the circular arc. Note that we have $\mathrm{d}\theta = u_c \mathrm{d}t$ along the circular arc, and the control along straight lines is zero. As a result, we have that the total control effort along the path is

$$J = \int_0^{t_f} u(t)^2\,\mathrm{d}t = \int_{\theta_0}^{\theta_f} u_c\,\mathrm{d}\theta = u_c|\theta_f - \theta_0| \\ = |\theta_f - \theta_0|/\rho \le 2\pi/\rho$$

This equation indicates that, for any small $\varepsilon > 0$, there exists $\rho > 0$ such that

$$\int_0^{t_f} u(t)^2\,\mathrm{d}t < \varepsilon$$

completing the proof.

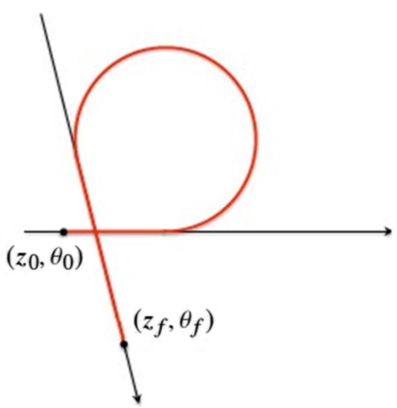

Fig. A1 Paths concatenated by circular arcs and straight lines.

Appendix B: Proof of Theorem 2

It is apparent that there exists at least one admissible trajectory of (Σ) from the initial condition $(x_0, 0, \theta_0)$ to the origin of Oxy such that the corresponding cost in Eq. (2) is finite; without loss of generality, let us assume that the finite cost is $\bar{J} > 0$. Note that we have

$$J = \int_0^{t_f} \kappa + (1-\kappa)\frac{1}{2}u^2(t)\,\mathrm{d}t \ge \kappa t_f$$

Given a fixed $\kappa \in (0, 1)$, this equation indicates that there exists $T > \bar{J}/\kappa$ such that every admissible controlled trajectory of (Σ) from $(x_0, 0, \theta_0)$ to the origin of Oxy will have a higher cost than $\bar{J}$ if the duration of the trajectory is greater than T. Therefore, in order to prove this theorem, we just need to prove that the OIP with its final time less than T has a solution.

Solving the OIP is equivalent to finding the elastica of a plane elastic curve (see Ref. [16]). According to Ref. [16] (Lemma 3), the curvature along the solution of the OIP has a global maximum, indicating that there exists $u_m > 0$ such that every measurable control $u(\cdot)$ on $[0, t_f]$ is not an optimal control of the OIP if there exists $\tau \in [0, t_f]$ such that $u(\tau) > u_m$. Therefore, we can consider that the set of admissible control is $[-u_m, u_m]$.

According to the preceding analyses, we just need to prove that a solution exists for the OIP where the final time is smaller than T, i.e., $t_f \le T$ and the control lies in $[-u_m, u_m]$. Let us consider an augmented system of (Σ) as

$$\dot{\boldsymbol{x}} = \boldsymbol{f}(\boldsymbol{x}, u) \tag{B1}$$

where $\boldsymbol{x} = [x, y, \theta, z]^T$, and

$$\boldsymbol{f}(x,u)=\begin{bmatrix}\cos\theta\\ \sin\theta\\ u\\ \kappa+(1-\kappa)\frac{1}{2}u^2\end{bmatrix}$$

It is clear that the problem of minimizing $z(t_f)$ subject to Eq. (B1) from $\boldsymbol{x}(0)=[x_0,0,\theta_0,0]$ to $[x(t_f),y(t_f)]=[0,0]$ has the same solution as the OIP. Hence, it amounts to proving that the new augmented optimal control problem has an optimum.

Let $\boldsymbol{x}_0$ be the initial condition of the augmented optimal control problem, i.e., $\boldsymbol{x}_0=(x_0,0,\theta_0,0)$. Let us denote by $\mathcal{A}_{x_0}(t)$ the attainable set of Eq. (B1) for time $t\geq 0$ from $\boldsymbol{x}_0$ with measurable locally bounded controls, i.e.,

$$\mathcal{A}_{x_0}(t)=\Big\{\boldsymbol{x}(t)=\boldsymbol{x}_0+\int_0^t \boldsymbol{f}(\boldsymbol{x}(t),u(t))\mathrm{d}t|x(0)=\boldsymbol{x}_0,\\ u\in L^\infty([0,t],[-u_m,u_m])\Big\}$$

With the definition of this attainable set, we denote by $\mathcal{A}_{x_0}^T$ the attainable sets for time not greater than T, i.e.,

$$\mathcal{A}_{x_0}^T=\bigcup_{0\leq t\leq T}\mathcal{A}_{x_0}(t)$$

Because $f(x,u)$ is bounded, the control set $[-u_m,u_m]$ is compact, and the set

$$\{\boldsymbol{f}(\boldsymbol{x},u)|u\in[-u_m,u_m]\}$$

is convex, it follows from Filippov's theorem (Ref. [17] corollary 10.6) that the attainable set $\mathcal{A}_{x_0}^T$ is compact. The compactness implies that there exists a time $\bar{t}\leq T$ and a point $(\bar{x}(\bar{t}),\bar{y}(\bar{t}),\bar{\theta}(\bar{t}),\bar{z}(\bar{t}))$ with $(\bar{x}(\bar{t}),\bar{y}(\bar{t}))=(0,0)$ such that $\bar{z}(\bar{t})$ is the minimum as compared with any other point $(x(t),y(t),\theta(t),z(t))\in\mathcal{A}_{x_0}^T$ with $(x(t),y(t))=(0,0)$ [see Ref. [17] proposition 10.2, in which $(\bar{x}(\bar{t}),\bar{y}(\bar{t}),\bar{\theta}(\bar{t}),\bar{z}(\bar{t}))$ lies on the boundary of $\mathcal{A}_{x_0}^T$]. By the definition of the attainable set $\mathcal{A}_{x_0}^T$, there exists an admissible control $u(\cdot):[0,\bar{t}]\to[-u_m,u_m]$ steering the system in Eq. (B1) from $\boldsymbol{x}_0$ to $(\bar{x}(\bar{t}),\bar{y}(\bar{t}),\bar{\theta}(\bar{t}),\bar{z}(\bar{t}))$, which completes the proof of Theorem 2.

Appendix C: Proofs for Lemmas

In this appendix, we present the proofs of all the lemmas established in the preceding text.

Proof of Lemma 1: Combining Eq. (16) with $H(t_f)=0$ to eliminate α, we obtain

$$\sin^2(\beta-\theta_f)-\sin(\beta-\theta_0)\sin(\beta-\theta_f)-\frac{\kappa}{2(1-\kappa)}(x_0\cos\beta)^2=0$$

Considering $\sin(\beta-\theta_f)=\kappa/\alpha(\beta)>0$, because of $H(t_f)=0$, we have

$$\sin(\beta-\theta_f)\\ =\frac{\sin(\beta-\theta_0)+\sqrt{\sin^2(\beta-\theta_0)+2\kappa(x_0\cos\beta)^2/(1-\kappa)}}{2}$$

Considering also $\sin(\beta-\theta_f)\leq 1$, we have

$$\frac{\sin(\theta_0-\beta)+\sqrt{\sin^2(\theta_0-\beta)+2\kappa(x_0\cos\beta)^2/(1-\kappa)}}{2}\leq 1$$

which is rewritten as

$$\sin(\theta_0-\beta)+2\geq\sqrt{\sin^2(\theta_0-\beta)+2\kappa(x_0\cos\beta)^2/(1-\kappa)}$$

Squaring both sides of this equation yields

$$\kappa x_0^2\cos^2\beta-2(1-\kappa)[\sin(\theta_0-\beta)+1]\leq 0 \tag{C1}$$

which completes the proof for Lemma 1.

Proof of Lemma 2: By contradiction, let us assume that there exists an interval $[t_1,t_2]\subset[0,t_f]$ (with $t_2\neq t_1$) such that $p_\theta(t)=0$ for $t\in[t_1,t_2]$. Then, the trajectory $(x(t),y(t))$ for $t\in[t_1,t_2]$ and the origin (0, 0) lie on the same straight line because $p_\theta(t)=p_xy(t)-p_yx(t)=0$ along the trajectory $(x(t),y(t))$ for $t\in[t_1,t_2]$ and at the origin (0, 0). In this case, the velocity or its opposite vector points to the origin, indicating

$$|\beta-\theta(t)|=\pi/2 \tag{C2}$$

for $t\in[t_1,t_2]$. According to Eq. (15), we have

$$p_\theta(t)=\pm\sqrt{2(1-\kappa)}\sqrt{\kappa-\alpha\sin(\beta-\theta(t))} \tag{C3}$$

for $t\in[0,t_f]$. Combining this equation with Eq. (C2) and taking into account $p_\theta(t)=0$ for $t\in[t_1,t_2]$ indicate $\kappa=\alpha$. This contradicts the hypothesis $\alpha(\beta^*)\neq\kappa$ of this lemma. Hence, it is impossible to have $p_\theta=0$ on a nonzero interval by contraposition.

Again by contradiction, let us assume that there exists an isolated instant $\tau\in(0,t_f)$ on the optimal trajectory of the OIP such that $p_\theta(\tau)=0$. If p_θ does not change its sign at τ, we have that the trajectory $(x(t),y(t))$ at τ is tangent to the straight line of $p_\theta=p_xy-p_yx=0$, indicating that the velocity or its opposite vector points to the origin. In this case, we also have $|\beta-\theta(\tau)|=\pi/2$, implying $\kappa=\alpha$ according to Eq. (C3) and $p_\theta(\tau)=0$. This contradicts the hypothesis of $\kappa\neq\alpha(\beta^*)$ once again. Hence, by contraposition, along an optimal trajectory of the OIP, it is impossible to have an isolated instant $\tau\in(0,t_f)$ such that $p_\theta(\tau)$ equals zero but p_θ does not change its sign at τ. Next, we shall prove that it is also impossible if p_θ changes its sign at τ.

1) If $\beta\in(-\pi/2,\pi/2)\cap\mathcal{S}$, we have $p_\theta(0)>0$ according to Eq. (14). As p_θ changes its sign at τ by assumption, the heading angle θ is monotonically nondecreasing before τ and monotonically nonincreasing after τ [recall the third equation of Eq. (1) and Eq. (5)]. Hence, the graph of (x,y) changes its sign of curvature at τ. For this scenario, there are two cases: either $y(\tau)>0$ or $y(\tau)<0$.

If $y(\tau)<0$, there must exist a point before τ so that the velocity at the point points to the origin, as illustrated by point A in Fig. C1. In this case, the dashed straight line is shorter and has less control effort than the solid trajectory after point A. So, the total solid trajectory cannot be optimal if $y(\tau)<0$.

Now, let us consider $y(\tau)>0$. According to Eqs. (20) and (6), we have $\sin(\beta-\theta(\tau))=\sin(\beta-\theta(t_f))$, which indicates that the angle between the velocity at τ and the vector from $(x(\tau),y(\tau))$ to $(0,0)$ is the same as that between the velocity at t_f and the vector from $(x(\tau),y(\tau))$ to $(0,0)$. As a result, the trajectory after τ must intersect, as illustrated by the curve in Fig. C2. In this case, there exist two points so that the straight line between the two points is tangent to the solid curve, as shown by points A and B in Fig. C2. In addition, there exists a point such that the line from the point to the origin is tangent to the solid curve, as shown by point C in Fig. C2. Then, the path from

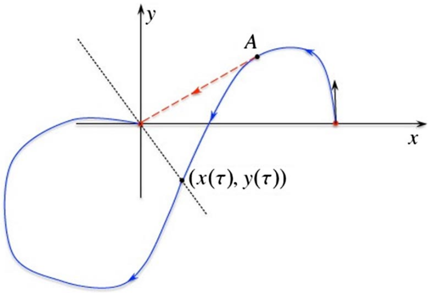

Fig. C1 Schematic path of (x,y) with $p_\theta(0)>0$ and $y(\tau)<0$ for the proof of Lemma 2.

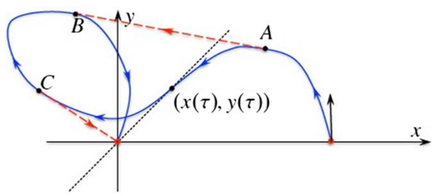

Fig. C2 Schematic path of (x,y) with $p_\theta(0) > 0$ and $y(\tau) > 0$ for the proof of Lemma 2.

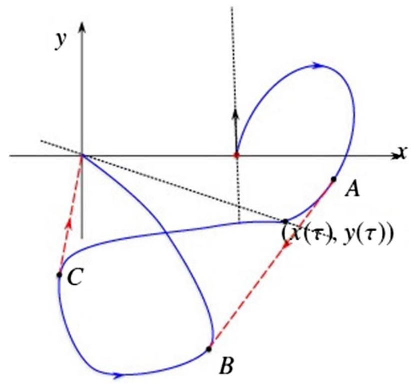

Fig. C3 Schematic path of (x,y) with $p_\theta(0) < 0$ and $y(\tau) < 0$ for the proof of Lemma 2.

initial point, passing points A, B, and C in order (and finally reaching to the origin), is shorter and has less control effort than the total solid curve. Therefore, the solid curve cannot be optimal if $y(\tau) > 0$. By contraposition, the first statement of this lemma is proved.

2) If $\beta \in (\pi/2, 3\pi/2) \cap \mathcal{S}$, we have $p_\theta(0) < 0$ according to Eq. (14). In this case, θ is monotonically nonincreasing before τ and monotonically nondecreasing after τ. Analogously, we have that either $y(\tau) < 0$ or $y(\tau) > 0$.

Analogous to proving the second case of the first statement, if $y(\tau) < 0$, the trajectory after τ must intersect, as shown by the solid line in Fig. C3. In this case, there exist two points so that the straight line between the two points tangent to the solid line, as shown by points A and B in Fig. C3. In addition, there exists a point so that the straight line from the point to the origin is tangent to the solid curve, as shown by point C in Fig. C3. Then, the path from the initial point, passing through points A, B, and C in order, and finally reaching to the origin, is shorter and has less control effort. So, the total solid trajectory is not optimal if $y(\tau) < 0$.

Now, let us consider the rest case $y(\tau) > 0$. Because the heading angle is monotonically nonincreasing for $t \in [0, \tau]$ and monotonically nondecreasing after τ, the shape of the trajectory is like the solid curve shown in Fig. C4. For such a trajectory, there exists a shorter smooth path from $(x_0, 0)$ with initial heading angle being θ_0 to a point A tangent to the solid curve, as shown by the dashed curve in Fig. C4. So, the solid curve is not the optimal path. Therefore, by contraposition, the second statement of this lemma is proved, which completes the whole proof of this lemma.

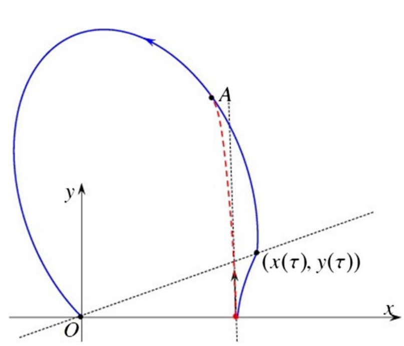

Fig. C4 Schematic path of (x,y) with $p_\theta(0) < 0$ and $y(\tau) > 0$ for the proof of Lemma 2.

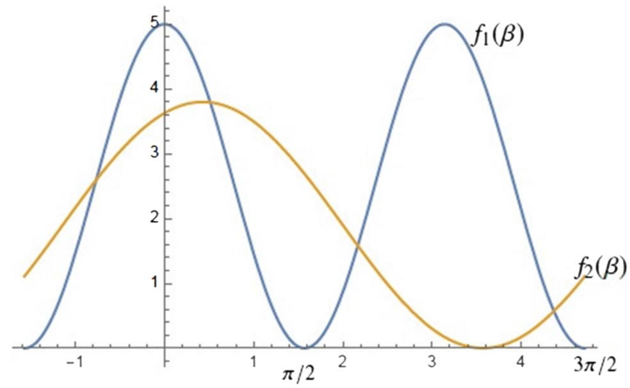

Fig. C5 Curves of $f_1(\beta)$ and $f_2(\beta)$ for $\beta \in (-\pi/2, 3\pi/2)$, $\kappa = 0.05$, $x_0 = 10$, and $\theta_0 = 2$.

Proof of Lemma 3. First of all, it is clear that $\theta_0 \in (\pi/2, \pi)$. In frame Oxy in Fig. 1, we have

$$\cos\sigma = -\frac{x\cos\theta + y\sin\theta}{\sqrt{x^2 + y^2}}$$

Hence, in order to guarantee $|\sigma| < \pi/2$, it requires us to keep

$$x(t)\cos\theta(t) + y(t)\sin\theta(t) < 0 \tag{C4}$$

along the solution of the OIP.

By contradiction, assume $\beta \in (\pi/2, 3\pi/2) \cap \mathcal{S}$. According to Corollary 1, we have that $\theta(t)$ is monotonically decreasing. Then, before reaching the target, there must exist a time $\tau \in (0, t_f)$ such that $\theta(\tau) = 0$ and $x(\tau) > 0$, indicating $x(\tau)\cos\theta(\tau) + y(\tau)\sin\theta(\tau) > 0$. This contradicts with Eq. (C4). Therefore, by contraposition, the proof is completed.

Proof of Lemma 4. According to Eqs. (6) and (14), and by the definition of $t_f(\beta)$, we have

$$p_\theta(t_f(\beta)) = \alpha(\beta)[x(t_f(\beta), \beta)\cos\beta + y(t_f(\beta), \beta)\sin\beta] = 0 \tag{C5}$$

Note that $\alpha(\beta) > 0$. For any $\beta \in \mathcal{S}$, if $y(t_f(\beta), \beta) = 0$, Eq. (C5) implies $x(t_f(\beta), \beta)\cos\beta = 0$. By the assumption of Lemma 4 that $|\beta| \neq \pi/2$, we finally have $x(t_f(\beta), \beta) = 0$, completing the proof.

Proof of Lemma 5. Because $\beta \neq |\pi/2|$, it is clear that M is strictly positive according to Eq. (31). Next, we prove the three statements of Lemma 5, one by one.

1) If $\kappa \leq M$, we must have

$$\kappa \leq \frac{2[\sin(\theta_0 - \beta) + 1]}{x_0^2\cos^2\beta + 2[\sin(\theta_0 - \beta) + 1]}$$

for any $\beta \in (-\pi/2, \pi/2)$. Then, by the definition of $\mathcal{S}$ in Eq. (18), the first statement holds.

2) Let $f_1(\beta) = \kappa x_0^2\cos^2\beta$ and $f_2(\beta) = 2(1-\kappa)[\sin(\theta_0 - \beta) + 1]$. Then, we have

$$\mathcal{S} = \{\beta \in \mathbb{S}: f_1(\beta) \leq f_2(\beta)\}$$

According to Eq. (31), if $\kappa > M$, there exists $\bar{\beta} \in (-\pi/2, \pi/2)$ such that $f_1(\bar{\beta}) > f_2(\bar{\beta})$, i.e., $\bar{\beta} \in \mathcal{S}$. For any $\theta_0 \in (0, \pi)$, we have $f_2(-\pi/2) > 0$ and $f_2(\pi/2) > 0$. However, $f_1(-\pi/2) = f_2(\pi/2) = 0$. As a result, in view of the mean value theorem, there exists $\beta_1 \in (-\pi/2, \bar{\beta})$ and $\beta_2 \in (\bar{\beta}, \pi/2)$ such that $f_1(\beta) \leq f_2(\beta)$ for $\beta \in (-\pi/2, \beta_1) \cup (\beta_2, \pi/2)$ and $f_1(\beta) > f_2(\beta)$ for $\beta \in (\beta_1, \beta_2)$, as demonstrated by the plot in Fig. C5.

In fact, as β_1 and β_2 are the boundary of $\mathcal{S}$, they must be two zeros of $f_1(\beta) = f_2(\beta)$, indicating

$$\kappa x_0^2\cos^2\beta - 2(1-\kappa)[\sin(\theta_0 - \beta) + 1] = 0 \tag{C6}$$

To solve this equation, let us consider

$$\cos\beta = \frac{1-\tan^2(\beta/2)}{1+\tan^2(\beta/2)} \text{ and } \sin\beta = \frac{2\tan(\beta/2)}{1+\tan^2(\beta/2)}$$

Substituting the two equations into Eq. (C6) leads to a fourth-degree polynomial in terms of $\tan(\beta/2)$:

$$\begin{aligned} 0 &= [\kappa x_0^2 - 2(1-\kappa)(1-\sin\theta_0)]\tan^4\left(\frac{\beta}{2}\right) \\ &+ 4(1-\kappa)\cos\theta_0 \tan^3\left(\frac{\beta}{2}\right) - 2[\kappa x_0^2 + 2(1-\kappa)]\tan^2\left(\frac{\beta}{2}\right) \\ &+ 4(1-\kappa)\cos\theta_0 \tan\left(\frac{\beta}{2}\right) + \kappa x_0^2 - 2(1-\kappa) \end{aligned} \tag{C7}$$

This indicates that $\tan(\beta_1/2)$ and $\tan(\beta_2/2)$ are two different zeros of the fourth-degree polynomial in Eq. (C7), completing the proof of the second statement of Lemma 5.

3) Note that $f_2(\pi/2) > 0$ and $f_2(3\pi/2) > 0$. However, for any $\theta_0 \in (0, \pi)$, there exists $\bar{\beta} \in (\pi/2, 3\pi/2)$ such that $f_2(\bar{\beta}) = 0$. Also, note that $f_1(\pi/2) = f_1(3\pi/2) = 0$. Therefore, according to the mean value theorem, there exists $\beta_3 \in (\pi/2, \bar{\beta})$ and $\beta_4 \in (\bar{\beta}, 3\pi/2)$ such that $f_1(\beta) \le f_2(\beta)$ for $\beta \in (\pi/2, \beta_3) \cup (\beta_4, 3\pi/2)$ and $f_1(\beta) > f_2(\beta)$ for $\beta \in (\beta_3, \beta_4)$, as demonstrated by Fig. C.5. According to the derivation procedure of Eq. (C7), we have that $\tan(\beta_3/2)$ and $\tan(\beta_4/2)$ are two zeros of Eq. (C7). Therefore, β_3 and β_4 can be obtained by solving the fourth-degree polynomial in Eq. (C7), completing the proof of the third statement of Lemma 5.

Acknowledgments

This research was supported by the Israel Science Foundation (grant no. 1469/15). The first author also acknowledges the support by the National Natural Science Foundation of China (grant no. 61703366).

References

[1] Bryson, A., "Linear Feedback Solutions for Minimum Effort Interceptions, Rendezvous and Soft Landing," *AIAA Journal*, Vol. 3, No. 8, 1965, pp. 1542–1544. doi:10.2514/3.3199

[2] Willems, G., "Optimal Controllers for Homing Missiles," U.S. Army Missiles Command TR RE-TR-68-15, Redstone Arsenal, AL, Sept. 1968.

[3] Cottrell, R. G., "Optimal Intercept Guidance for Short-Range Tactical Missiles," *AIAA Journal*, Vol. 9, No. 7, 1971, pp. 1414–1415. doi:10.2514/3.6369

[4] Anderson, G. M., "Effects of Performance Index/Constraint Combinations on Optimal Guidance Laws for Air-to-Air Missiles," *Proceedings, NAECON'79*, IEEE Publ., Piscataway, NJ, 1979, pp. 765–771.

[5] Anderson, G. M., "Comparison of Optimal Control and Differential Game Intercept Missile Guidance," *Journal of Guidance, Control, and Dynamics*, Vol. 4, No. 2, 1981, pp. 109–115. doi:10.2514/3.56061

[6] Kreindler, E., "Optimality of Proportional Navigation," *AIAA Journal*, Vol. 11, No. 6, 1973, pp. 878–880. doi:10.2514/3.50527

[7] Bryson, A. E., and Ho, Y. C., *Applied Optimal Control*, Hemisphere, Washington, D.C., 1975, pp. 154–155.

[8] Lu, P., and Chavez, F. R., "Nonlinear Optimal Guidance," *AIAA Guidance, Navigation, and Control Conferences and Exhibit*, AIAA Paper 2006-6079, 2006, pp. 0–11. doi:10.2514/6.2006-6079

[9] Jeon, I., and Lee, J., "Optimality of Proportional Navigation Based on Nonlinear Formulation," *IEEE Transactions on Aerospace and Electronic Systems*, Vol. 46, No. 4, 2010, pp. 2051–2055. doi:10.1109/TAES.2010.5595614

[10] Guelman, M., and Shinar, J., "Optimal Guidance Law in the Plane," *Journal of Guidance, Control, and Dynamics*, Vol. 7, No. 4, 1984, pp. 471–476. doi:10.2514/3.19880

[11] Sim, Y. C., Leng, S. B., and Subramaniam, V., "An All-Aspect Near-Optimal Guidance Law," *Dynamics and Control*, Vol. 10, No. 2, 2000, pp. 165–177. doi:10.1023/A:1008395924656

[12] Liu, X., Shen, Z., and Lu, P., "Closed-Loop Optimization of Guidance Gain for Constrained Impact," *Journal of Guidance, Control, and Dynamics*, Vol. 40, No. 2, 2017, pp. 453–460. doi:10.2514/1.G000323

[13] Pontryagin, L. S., Boltyanski, V. G., Gamkrelidze, R. V., and Mishchenko, E. F., *The Mathematical Theory of Optimal Processes*, Interscience, New York, 1962 (translated from Russian).

[14] Becker, K., "Closed-Form Solution of Pure Proportional Navigation," *IEEE Transactions on Aerospace and Electronic Systems*, Vol. 26, No. 3, 1990, pp. 526–533. doi:10.1109/7.106131

[15] Arfken, G., "Elliptic Integrals," *Mathematical Methods for Physicists*, 3rd ed., Academic Press, Orlando, FL, 1985, pp. 321–327.

[16] Brunnett, G., "The Curvature of Plane Elastic Curves," Naval Postgraduate School TR NPS-MA-93-013, March 1993, https://calhoun.nps.edu/handle/10945/28706.

[17] Agrachev, A., and Sachkov, Y., *Control Theory from the Geometric Viewpoint*, Springer, Berlin, 2004.